

An extremely brief end Ordovician mass extinction linked to abrupt onset of glaciation

Ming-Xing Ling ^{a,*}, Ren-Bin Zhan ^{b,c,**}, Guang-Xu Wang ^b, Yi Wang ^b, Yuri Amelin ^d, Peng Tang ^b, Jian-Bo Liu ^e, Jisuo Jin ^f, Bing Huang ^b, Rong-Chang Wu ^b, Shuo Xue ^{a,c}, Bin Fu ^d, Vickie C. Bennett ^d, Xin Wei ^b, Xiao-Cong Luan ^b, Seth Finnegan ^g, David A.T. Harper ^h, Jia-Yu Rong ^b

^a State Key Laboratory of Isotope Geochemistry, Guangzhou Institute of Geochemistry, Chinese Academy of Sciences, Guangzhou 510640, China

^b State Key Laboratory of Palaeobiology and Stratigraphy, Center for Excellence in Life and Paleoenvironment, Nanjing Institute of Geology and Palaeontology, Chinese Academy of Sciences, 39 East Beijing Road, Nanjing 210008, China

^c University of Chinese Academy of Sciences, Beijing 100094, China

^d Research School of Earth Sciences, Australian National University, Canberra, ACT 0200, Australia

^e School of Earth and Space Sciences, Peking University, Beijing 100871, China

^f Department of Earth Sciences, University of Western Ontario, London, ON N6A 5B7, Canada

^g Department of Integrative Biology, University of California, Berkeley, CA, USA

^h Palaeoecosystems Group, Department of Earth Sciences, Durham University, Durham DH1 3LE, UK

Received 8 November 2019; revised 10 November 2019; accepted 10 November 2019

Available online 9 December 2019

Abstract

The end Ordovician mass extinction (EOME) was the second most severe biotic crisis in Phanerozoic, and has been widely linked to a major glaciation. However, robust geochronology of this interval is still lacking. Here we present four successive high-precision zircon U–Pb dates by isotope dilution thermal ionization mass spectrometry (ID-TIMS) for biostratigraphically well-constrained K-bentonites of a continuous Ordovician-Silurian boundary section at Wanhe, SW China. They include 444.65 ± 0.22 Ma (middle *Dicellograptus complexus* Biozone), 444.06 ± 0.20 Ma (lower *Paraorthograptus pacificus* Biozone), 443.81 ± 0.24 Ma (upper *Tangyagraptus typicus* Subzone), and 442.99 ± 0.17 Ma (upper *Metabolograptus extraordinarius* Biozone). Calculations based on sedimentation rates suggest a duration of 0.47 ± 0.34 Ma for the Hirnantian Stage, which is much shorter than previously thought (1.4 ± 2.05 Ma in the International Chronostratigraphic Chart ver. 2019/05). The new data also constrain the Hirnantian glacial maximum to ~ 0.2 Ma, supporting that its brevity and intensity probably triggered the EOME.

Copyright © 2019, Guangzhou Institute of Geochemistry. Production and hosting by Elsevier B.V. This is an open access article under the CC BY-NC-ND license (<http://creativecommons.org/licenses/by-nc-nd/4.0/>).

Keywords: ID-TIMS; K-bentonite; End Ordovician mass extinction (EOME); Hirnantian stage

1. Introduction

* Corresponding author.

** Corresponding author. State Key Laboratory of Palaeobiology and Stratigraphy, Center for Excellence in Life and Paleoenvironment, Nanjing Institute of Geology and Palaeontology, Chinese Academy of Sciences, 39 East Beijing Road, Nanjing 210008, China.

E-mail addresses: mxling@gig.ac.cn (M.-X. Ling), rbzhan@nigpas.ac.cn (R.-B. Zhan).

Peer review under responsibility of Guangzhou Institute of Geochemistry.

The Ordovician-Silurian boundary interval witnessed one of the major glaciation and the second largest biotic crisis in the Phanerozoic, i.e., the end Ordovician mass extinction (EOME) (Sheehan, 2001; Brenchley et al., 2003; Harper et al., 2014; Wang et al., 2019). The EOME was the first of the Phanerozoic “big five” mass extinctions (Raup and Sepkoski,

1982; Sepkoski, 1996) and has been widely linked to the Late Ordovician glaciation (Sheehan, 2001; Finnegan et al., 2012); however, consensus on its timing and tempo, and hence the causal mechanism, has not been achieved. One reason is the lack of precise geochronological constraints on this crucial time interval. The current geochronology of this interval was actually calibrated by the CONOP program on the basis of very sparse radiogenic isotope dates in low precision (up to ~1%), which were yielded from multiple zircon grains, thus producing relatively large uncertainties (Cooper and Sadler, 2012; Ogg et al., 2016). A group in Chinese Academy Sciences dated the K-bentonite from the top of the Kuanyinchiao Formation at Wangjiawan North section, the Global Stratotype Section and Point (GSSP) of the Hirnantian Stage, using sensitive high resolution ion microprobe (SHRIMP) and achieved a boundary age of 443.2 ± 1.6 Ma (Hu et al., 2008).

Here we present high-precision isotope dilution thermal ionization mass spectrometry (ID-TIMS) zircon dating of K-bentonite beds from a newly discovered Ordovician-Silurian boundary section in northeastern Yunnan, South China (Tang et al., 2017). The new dates provide new high-resolution geochronological constraints of the Hirnantian Stage, and also contribute to our understanding of the timing and tempo of the EOME and its subsequent recovery during this time interval.

2. Geological setting and samples

During the Late Ordovician, South China straddled the equator (Jin et al., 2018). Much of the South China paleoplate was covered by a restricted epicontinent sea and received organic-rich mud deposits that became the black shale sequence of the Wufeng Formation. At some near-shore localities in the southwestern part of the Yangtze Platform, argillaceous limestone layers developed with intercalated graptolitic black shales, forming the Daduhe Formation of this study.

At Wanhe, the Daduhe Formation, 24.3 m thick, conformably overlies the Linhsiang Formation (lower Katian, Upper Ordovician) (Fig. 1). It contains a number of K-bentonite beds, with a thickness ranging from 1–2 mm to several centimeters. Five successive graptolite biozones from upper Katian to lower Hirnantian are recognized in the Daduhe Formation, which are readily correlative to those in the widespread Wufeng Formation on the Yangtze Platform (see Fig. 2 for details). The overlying Kuanyinchiao Formation is 50 cm thick and yields the typical *Hirnantia* brachiopod fauna that has a worldwide distribution and is largely confined to the lower Hirnantian, providing further biostratigraphic constraint on these K-bentonite beds. The sedimentological and biostratigraphical features indicate a continuous sedimentary succession without any detectable hiatuses after our millimeter-scale observation and measurements, and make the Daduhe Formation ideally suited for geochronological calibrations.

Totally, 23 layers of K-bentonites were sampled from the section ranging from the Daduhe Formation to the base of the

Lungmachi Formation, amongst which zircons were successfully separated from 18 samples, with a number of grains ranging from several to around one thousand. Possibility of field contamination was excluded, as all the samples were collected with special caution in the field to avoid contamination from its underlying and overlying layers, all of which were packed in vacuum plastic bags separately.

3. Analytical methods

Zircon separation, annealing, ion microprobe analysis, chemical abrasion, column chemistry and ID-TIMS analysis were conducted in the Research School of Earth Sciences, Australian National University, with all chemical procedures carried out in ultra-clean laboratory (The famous SPIDER² laboratory). Zircon grains were extracted by crushing, magnetic, and heavy liquid separation techniques and were hand-picked under a binocular microscope. Zircon grains were transferred to quartz vials and then put into furnace for annealing at 900 °C for 48 h, which helped restore the crystallinity of the zircon crystals that experienced light to moderate radiation damage (Mattinson, 2005; Huyskens et al., 2016).

The zircon grains were mounted in epoxy and then slightly polished for Cathodoluminescence (CL) imaging and preliminary SHRIMP analysis, to facilitate the selection of best grains for ID-TIMS analysis. SHRIMP dating indicated that some samples had severe problem of inheritance from preceding stratigraphy and were not suitable for dating volcanic events.

Subsequently, the zircon grains were transferred from the mount to Teflon beakers filled with HF, put in Teflon liner and assembled in Parr bomb for chemical abrasion (leaching) at 190 °C for 15 h. Chemical abrasion removes parts of the crystals that suffered from strong radiation damage and most likely experienced Pb loss, at conditions where the crystalline zircon does not dissolve (Mattinson, 2005; Huyskens et al., 2016). Then the individual zircon grains were transferred into microcapsules filled with HF and a ^{202}Pb – ^{205}Pb – ^{233}U – ^{236}U spike for dissolving at 220 °C for at least 72 h. The sample dissolutions were converted to chlorides using 2.5 M HCl and moved on for column chemistry, in which U and Pb were eluted by 0.5 M HNO₃. Finally the U–Pb cuts were loaded on outgassed zone refined Re-filaments (99.999% Re, H. Cross Company), with silicagel and isotope ratios were analysed using Triton Plus (Huyskens et al., 2012). Standards including Temora zircon and EARTHTIME solutions were also analysed to monitor the data quality.

Isotopic results for the samples and standards are presented in Table 1. The isotopic ratios were corrected for common Pb, instrumental mass fractionation and spike. The U–Pb dates and uncertainties were calculated using the algorithms of Schmitz and Schoene (2007), with the decay constants proposed by Jaffey et al. (1971), Villa et al. (2016) and a $^{238}\text{U}/^{235}\text{U}$ ratio of 137.818 (Hiess et al., 2012). The weighted

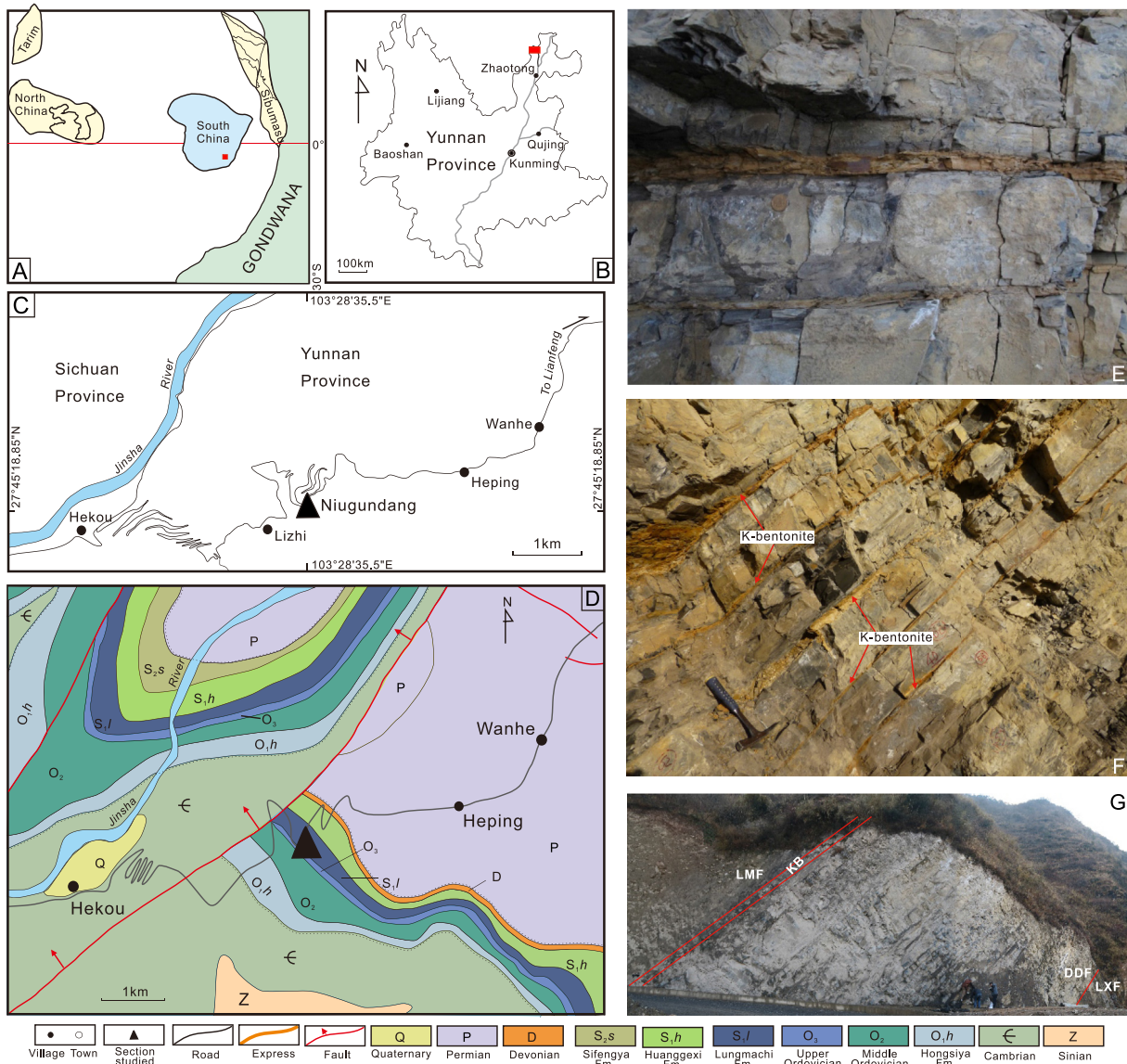


Fig. 1. Locality and geologic setting of the study section. A, paleogeographic position of South China during the Late Ordovician. B, geographic map of Yunnan Province, SW China, with a small red rectangle showing the position of C. C, location map of the section studied in this study. D, simplified geologic map of the study area with a solid triangle showing the exact locality of the studied section. E-G, bird's-eye view (G) of the section and close-up views (E, F) of the Daduhe Formation showing its lithology and those intercalated K-bentonites. B, C and D are cited from Tang et al. (2017).

mean dates of $^{206}\text{Pb}/^{238}\text{U}$ were calculated by Isoplot (Ludwig, 2012). The errors are documented in 2 sigma.

4. Results

Only a few zircon grains of 4 samples (AGM72, AGM104, AGM107A, AGM120) were finally proceeded for ID-TIMS U–Pb isotopic dating and yielded high precision results (Table 1). Graptolite zonation through a continuous stratigraphic section provides a biostratigraphic context for the four samples. These include AGM72 (middle *Dicellograptus complexus* Biozone), AGM104 (lower *Paraorthograptus pacificus* Biozone), AGM107A (upper *Tangyagraptus typicus* Subzone, 3.23 m below the base of the Hirnantian Stage) and AGM120 (upper *Metabolograptus extraordinarius* Biozone, 1.04 m above the base of the Hirnantian Stage).

The four K-bentonite samples (AGM72, AGM104, AGM107A and AGM120, see Fig. 2 for detailed horizons) yielded weighted mean $^{206}\text{Pb}/^{238}\text{U}$ dates of 444.65 ± 0.22 Ma ($n = 7$, MSWD = 1.2), 444.06 ± 0.20 Ma ($n = 3$, MSWD = 2.8), 443.81 ± 0.24 Ma ($n = 4$, MSWD = 2.1) and 442.99 ± 0.17 Ma ($n = 5$, MSWD = 1.12), respectively (Figs. 2 and 3). The Temora zircon and EARTHTIME standard solutions show consistent $^{206}\text{Pb}/^{238}\text{U}$ dates (Table 1), similar to the values reported in other recent geochronological studies.

5. Calibrating numerical ages of major chronostratigraphic boundaries

Using the four ID-TIMS zircon U–Pb dates as controlling points, an improved estimate of numerical ages of chronostratigraphic boundaries can be reached by calculating the

Table 1
Zircon U–Pb isotopic results analysed by ID-TIMS.

Sample	Compositional Parameters										Radiogenic Isotope Ratios										Isotopic ages							
	Th/U	$^{206}\text{Pb}^*$ $\times 10^{-13}$	mol %	Pb*/ $^{206}\text{Pb}^*$	Pbc	$^{206}\text{Pb}/^{204}\text{Pb}$	$^{208}\text{Pb}/^{206}\text{Pb}$	$^{207}\text{Pb}/^{206}\text{Pb}$	% err	$^{207}\text{Pb}/^{235}\text{U}$	% err	$^{206}\text{Pb}/^{238}\text{U}$	% err	corr. coef.	$^{207}\text{Pb}/^{206}\text{Pb}$	±	$^{207}\text{Pb}/^{235}\text{U}$	±	$^{206}\text{Pb}/^{238}\text{U}$	±								
	(a)	(b)	(c)	(c)	(c)	(d)	(e)	(e)	(f)	(e)	(f)	(e)	(f)	(g)	(f)	(g)	(f)	(g)	(f)									
AGM120-1	0.7577751	0.5065486	98.80%	27	0.51	1524	0.2382473	0.0559164	0.6914604	0.5482227	0.6368381	0.0711397	0.0800851	-0.6484269	448.05	15.36	443.83	2.29	443.02	0.34								
AGM120-2	0.6872139	0.3239737	97.39%	12	0.71	706	0.2159149	0.0558765	1.1045294	0.5481475	1.018062	0.0711807	0.1268466	-0.6483184	446.46	24.55	443.78	3.66	443.27	0.54								
AGM120-3	0.5425901	1.037265	99.39%	50	0.53	2969	0.1707979	0.0559923	0.279868	0.5487356	0.3098484	0.0711097	0.0555438	0.6032789	451.07	6.21	444.17	1.11	442.84	0.24								
AGM120-4	0.5992994	0.3000954	98.61%	22	0.35	1299	0.1886393	0.0560012	0.9495927	0.5493616	1.0408596	0.0711795	0.1049242	0.8821045	451.42	21.09	444.58	3.75	443.26	0.45								
AGM120-5	0.7421202	0.4291945	98.20%	18	0.65	1017	0.2340044	0.0561214	0.7316461	0.5505095	0.8161751	0.0711755	0.1922594	0.534675	456.18	16.23	445.33	2.94	443.23	0.82								
AGM107A-1	0.5933789	0.3298318	97.91%	15	0.58	880	0.1869465	0.0560706	1.0657156	0.5503431	0.9832895	0.0712185	0.105844	-0.75757	454.17	23.65	445.22	3.54	443.49	0.45								
AGM107A-2	0.6199785	0.2706917	97.54%	12	0.56	746	0.1950444	0.0559727	1.3006466	0.5494281	1.2000311	0.0712243	0.1195517	-0.827077	450.29	28.89	444.62	4.32	443.53	0.51								
AGM107A-3	0.6312201	0.3059044	98.36%	19	0.42	1110	0.1984539	0.0559441	1.1247093	0.5498168	1.0381389	0.0713112	0.1218611	-0.681331	449.15	24.98	444.88	3.74	444.05	0.52								
AGM107A-4	0.6195733	0.3525198	98.60%	22	0.41	1302	0.1948072	0.055952	0.9823334	0.5500108	0.9065396	0.0713263	0.1015032	-0.7219447	449.46	21.82	445.00	3.27	444.14	0.44								
AGM104-1	0.8827781	1.3451922	98.80%	28	1.33	1518	0.2775732	0.0559485	0.3177966	0.5496652	0.349449	0.0712859	0.059017	0.5964795	449.33	7.06	444.78	1.26	443.90	0.25								
AGM104-2	1.0748942	0.682094	99.35%	54	0.37	2782	0.33849	0.0560637	0.2590322	0.5512896	0.2963273	0.0713496	0.0932638	0.5320898	453.89	5.75	445.84	1.07	444.28	0.40								
AGM104-3	0.5592262	0.3509552	98.14%	16	0.54	983	0.1762232	0.0561176	0.5386045	0.5522639	0.6048286	0.0714071	0.1615262	0.5210753	456.03	11.95	446.48	2.18	444.63	0.69								
AGM72-1	0.6531772	0.5471432	98.85%	27	0.52	1591	0.2054946	0.0559984	0.3480821	0.5507238	0.3921661	0.0713595	0.1091268	0.5203983	451.31	7.73	445.47	1.41	444.34	0.47								
AGM72-2	0.6389754	0.3314506	98.18%	17	0.50	1003	0.2013752	0.0561176	0.5743918	0.5519183	0.6367184	0.0713625	0.1367259	0.5409078	456.03	12.74	446.25	2.30	444.36	0.59								
AGM72-3	0.7710114	0.3049707	97.19%	11	0.72	653	0.2438689	0.0563696	0.5792493	0.5544888	0.6397297	0.0713743	0.129215	0.5469268	465.96	12.83	447.93	2.32	444.43	0.55								
AGM72-4	0.7521127	0.4243925	98.50%	21	0.53	1218	0.2372139	0.0561847	0.4211503	0.5531736	0.4769309	0.0714394	0.1381397	0.5250064	458.68	9.34	447.07	1.72	444.82	0.59								
AGM72-5	0.6600377	0.1787229	97.59%	13	0.36	750	0.2084948	0.0562945	0.9759071	0.5544457	1.0693961	0.071464	0.1382719	0.7112199	463.00	21.63	447.90	3.87	444.97	0.59								
AGM72-6	0.7617539	0.6519554	98.47%	21	0.83	1202	0.2397311	0.0560409	0.4695819	0.5520176	0.5288939	0.071473	0.161159	0.4997527	452.99	10.42	446.32	1.91	445.02	0.69								
AGM72-7	0.7001424	0.3636643	98.70%	24	0.39	1389	0.2207665	0.0561739	0.4889781	0.5533741	0.5544637	0.071479	0.1603004	0.5289482	458.25	10.84	447.20	2.01	445.06	0.69								
ET100	0.0739579	1.5811013	99.84%	168	0.21	11,132	0.0236349	0.0479938	0.2521661	0.1037569	0.2350358	0.0156865	0.0489821	-0.2582703	97.90	5.96	100.24	0.22	100.34	0.05								
ET100 ZN088	0.0740282	1.5453812	99.75%	109	0.31	7272	0.0237216	0.0481292	0.2209573	0.104	0.2467402	0.015679	0.065592	0.5054594	104.56	5.22	100.46	0.24	100.29	0.07								
ET100 ZN-060	0.0725212	1.5442476	99.76%	113	0.30	7557	0.0231307	0.0478935	0.2426776	0.1034242	0.2751697	0.015669	0.0888034	0.5056471	92.94	5.75	99.93	0.26	100.23	0.09								
ET100 ZN-102	0.0726802	1.7389522	99.64%	74	0.52	5041	0.023185	0.0479029	0.1964659	0.1035191	0.2164454	0.0156803	0.0465361	0.517018	93.41	4.65	100.02	0.21	100.30	0.05								
ET100 ZN-103	0.0732254	1.7392453	99.67%	81	0.48	5476	0.0233961	0.0479826	0.192304	0.1036796	0.2105074	0.0156785	0.0377932	0.5505999	97.35	4.55	100.17	0.20	100.29	0.04								
ET100 ZN-061	0.0733746	1.7047478	99.80%	136	0.28	9062	0.0234191	0.0479323	0.2035019	0.1036901	0.2336032	0.0156965	0.0816066	0.5197633	94.86	4.82	100.18	0.22	100.40	0.08								
ET250	0.0775848	1.4363508	99.84%	168	0.19	10,998	0.0261592	0.0549344	0.2471812	0.301731	0.2320698	0.0398538	0.0610588	-0.1239937	408.55	5.53	267.75	0.55	251.93	0.15								
ET250	0.0777278	1.4366812	99.84%	174	0.18	11,365	0.0262256	0.0549802	0.2462364	0.3020928	0.2270685	0.0398684	0.0471362	-0.3200186	410.41	5.51	268.03	0.53	252.02	0.12								
ET250	0.0771778	1.4448784	99.80%	139	0.23	9062	0.0260195	0.0549304	0.2030794	0.3017935	0.2279302	0.0398649	0.0556576	0.544247	408.39	4.54	267.80	0.54	252.00	0.14								
ET250	0.0777722	1.2695006	99.70%	92	0.31	6074	0.0262622	0.0550276	0.2310703	0.302193	0.2638544	0.0398472	0.0799633	0.5360473	412.34	5.17	268.11	0.62	251.89	0.20								
ET250	0.0779803	1.269627	99.71%	93	0.30	6179	0.0263623	0.0551003	0.2272795	0.3026884	0.2604288	0.0398598	0.0810596	0.5385492	415.29	5.08	268.50	0.61	251.96	0.20								
ET250	0.0779851	1.3485803	99.80%	133	0.23	8685	0.0263437	0.055056	0.2184069	0.3025976	0.2487212	0.03988	0.073336	0.5355977	413.49	4.88	268.43	0.59	252.09	0.18								
ET250	0.0776429	1.334061	99.79%	131	0.23	8560	0.0261861	0.0549634	0.2163661	0.302388	0.2460224	0.0399195	0.0706862	0.5379204	409.73	4.84	268.26	0.58	252.33	0.17								
ET250	0.067554	1.4488453	99.81%	142	0.23	9289	0.0227739	0.0549291	0.1974136	0.3018564	0.2186859	0.0398742	0.0393862	0.603878	408.33	4.42	267.85	0.51	252.05	0.10								
ET500	0.0866139	1.2711877	99.73%	100	0.28	6632	0.0270977	0.0572687	0.2695845	0.6377338	0.2477198	0.0808009	0.0486887	-0.3706154	500.90	5.94	500.90	0.98	500.90	0.23								
ET500	0.0864054	1.270949	99.72%	97	0.29	6449	0.027017	0.0572251	0.2686072	0.6371325	0.246822	0.0807863	0.0533007	-0.3187854	499.23	5.92	500.53	0.98	500.81	0.26								
ET500	0.086899	1.1959898	99.60%	69	0.39	4581	0.0272257	0.0573501	0.2337541	0.6377139	0.2624688	0.0806837	0.0606925	0.5628557	504.03	5.14	500.89	1.04	500.20	0.29								
ET500	0.0870557	1.445146	99.70%	90	0.36	5616	0.0272641	0.0573247	0.2646417	0.6375464	0.2932292	0.0806983	0.0533257	0.6008896	503.05	5.82	500.79	1.16	500.29	0.26								
ET500	0.0869346	1.4450735	99.71%	94	0.34	5866	0.0272125	0.0572952	0.2600567	0.6375136	0.2904212	0.0807357	0.0637144	0.561352	501.92	5.72	500.77	1.15	500.51	0.31								
ET500	0.0872305	1.3831452	99.69%	87	0.36	5784	0.0273527	0.0574318	0.213891	0.6395413	0.2559231	0.0807998	0.1056362	0.571603	507.16	4.70	502.02	1.01	500.90	0.51								
ET500	0.085681	1.3109094	99.68%	84	0.35																							

Table 1 (continued)

Sample	Compositional Parameters										Radiogenic Isotope Ratios							Isotopic ages						
	Th/U	$^{206}\text{Pb}^*$ $\times 10^{-13}$	mol %	Pb^*/Pbc	$^{206}\text{Pb}/\text{Pbc}$	$^{208}\text{Pb}/^{206}\text{Pb}$	$^{207}\text{Pb}/^{206}\text{Pb}$	% err	$^{207}\text{Pb}/^{235}\text{U}$	% err	$^{206}\text{Pb}/^{238}\text{U}$	% err	corr. coef.	$^{207}\text{Pb}/\text{Pb}$	\pm	$^{206}\text{Pb}/\text{U}$	\pm	$^{206}\text{Pb}/\text{U}$	\pm	$^{206}\text{Pb}/\text{U}$	\pm			
(a)	(b)	(c)	(c)	(c)	(d)	(e)	(e)	(f)	(e)	(f)	(e)	(g)	(f)	(g)	(f)	(g)	(f)	(g)	(f)	(g)	(f)	(g)		
Temora	0.3850929	0.8240648	99.36%	46	0.44	2827	0.1212838	0.05553093	0.3476818	0.5104472	0.3831606	0.0669648	0.057898	0.6559638	423.74	7.76	418.75	1.31	417.84	0.23				
Temora	0.4924247	4.4477946	99.90%	309	0.36	18.352	0.1552687	0.05552711	0.1233857	0.5049205	0.16044957	0.06622856	0.0878416	0.64772809	422.20	2.75	415.03	0.55	413.74	0.35				
Temora	0.2704876	5.1779462	99.88%	244	0.50	15.524	0.0850291	0.0551815	0.1155746	0.5091931	0.1504051	0.066955	0.0837444	0.6507299	418.58	2.57	417.91	0.52	417.78	0.34				
Temora	0.431687	0.4769321	97.31%	11	1.08	669	0.13673	0.0556904	0.8969518	0.5140246	0.978644	0.0669726	0.1070965	0.7856699	439.05	19.96	421.15	3.37	417.89	0.43				
Temora	0.4914813	1.3191048	99.06%	32	1.03	1905	0.1550664	0.0554227	0.3311349	0.5112147	0.3709834	0.0669283	0.0941275	0.5274713	428.31	7.38	419.27	1.27	417.62	0.38				
Temora	0.2761163	5.3127481	99.89%	259	0.48	16.516	0.0867729	0.0551549	0.1301608	0.5086371	0.1233491	0.0669142	0.0504813	0.0659684	417.50	2.91	417.53	0.42	417.54	0.20				

(a) 1,2 etc. are labels for fractions composed of single zircon grains or fragments; all fractions annealed for 48 h at 900 °C and chemically abraded at 190 °C after Mattinson (2005).

(b) Model Th/U ratio calculated from radiogenic $^{208}\text{Pb}/^{206}\text{Pb}$ ratio and $^{207}\text{Pb}/^{235}\text{U}$ age.(c) Pb* and Pbc represent radiogenic and common Pb, respectively; mol % $^{206}\text{Pb}^*$ with respect to radiogenic, blank and initial common Pb.

(d) Measured ratio corrected for spike and fractionation only.

(e) Corrected for fractionation, spike, and common Pb; all non-radiogenic Pb was assumed to be procedural blank with a composition of $^{206}\text{Pb}/^{204}\text{Pb} = 16.96 \pm 0.35$; $^{207}\text{Pb}/^{204}\text{Pb} = 14.48 \pm 0.29$; $^{208}\text{Pb}/^{204}\text{Pb} = 35.03 \pm 0.7$ (all uncertainties 2-sigma) for up to 0.4 pg. Any excess was assumed to be modern day crustal Pb after Stacey and Kramers (1975).

(f) Errors are 2-sigma, propagated using the algorithms of Schmitz and Schoene (2007).

(g) Calculations are based on the decay constants of Jaffey et al. (1971) and a $^{238}\text{U}/^{235}\text{U}$ ratio of 137.818 (Hiess et al., 2012). $^{206}\text{Pb}/^{238}\text{U}$ and $^{207}\text{Pb}/^{206}\text{Pb}$ ages corrected for initial disequilibrium in $^{230}\text{Th}/^{238}\text{U}$ using Th/U [magma] = 3.

sedimentation rates of different lithofacies (carbonate and mudstone/shale) against the fine graptolite biozones at the section of this study and the Hirnantian Stage GSSP standard zonation in Yichang (Hubei, central China).

The numerical ages of major chronostratigraphic boundaries include: the O–S boundary (442.67 ± 0.24 Ma); the *Hirnantia* Fauna/the Kuanyinchiao Formation (442.96 ± 0.17 Ma to 442.92 ± 0.17 Ma); the base of the Hirnantian Stage (443.14 ± 0.24 Ma); the base of *Dicellograptus mirus* Subzone (443.41 ± 0.24 Ma); the base of the *T. typicus* Subzone (444.17 ± 0.28 Ma); the base of the *P. pacificus* Biozone (444.38 ± 0.31 Ma); and the base of the *D. complexus* Biozone (444.84 ± 0.31 Ma) (Fig. 2, Table 2). Average sedimentation rates calculated based on different lithofacies indicate a general decrease up-section, from 21.93 m/Ma to 4.73 m/Ma, but increased in the Kuanyinchiao Formation (12.58 m/Ma).

Calculation procedures are documented below in details.

(1) Calculating the average sedimentation rates with the ID-TIMS zircon U–Pb dates as reference points: The average sedimentation rate (m/Ma) for the successions from AGM72 to AGM104, from AGM 104 to AGM107A, and from AGM107A to AGM120 were calculated using thickness (m) divided by duration (Ma) without adjustment of compaction of soft sediments during diagenesis.

$$R_{ave} = T/D$$

where R is sedimentation rate (m/Ma), T is accumulated thickness (m) of the interval, and D (Ma) is duration of the interval.

(2) Calculating the sedimentation rates of different lithofacies: Based on lithofacies analysis, two major lithofacies, limestone (argillaceous limestone/skeletal wackestone) and mudstone (mudstone/shale) were distinguished. The sedimentation rates of limestone and mudstone were calculated by using the accumulative thickness of each lithofacies between AGM72 and AGM104, AGM104 and AGM107A, as well as ID-TIMS zircon U–Pb dates of AGM72, AGM104 and AGM107A.

$$T1_{mud}/R1_{mud} + T1_{lim}/R1_{lim} = D1$$

$$T2_{mud}/R1_{mud} + T2_{lim}/R1_{lim} = D2$$

where $T1_{mud}$, $T1_{lim}$, $T2_{mud}$ and $T2_{lim}$ T are accumulated thickness (m) of the interval for mudstone and limestone between AGM72 and AGM104, AGM104 and AGM107A, respectively. $R1_{mud}$ and $R1_{lim}$ are sedimentation rates (m/Ma) of mudstone and limestone between AGM72 and AGM107A, respectively. D1 and D2 are duration (Ma) between AGM72 and AGM104, AGM104 and AGM107A, respectively.

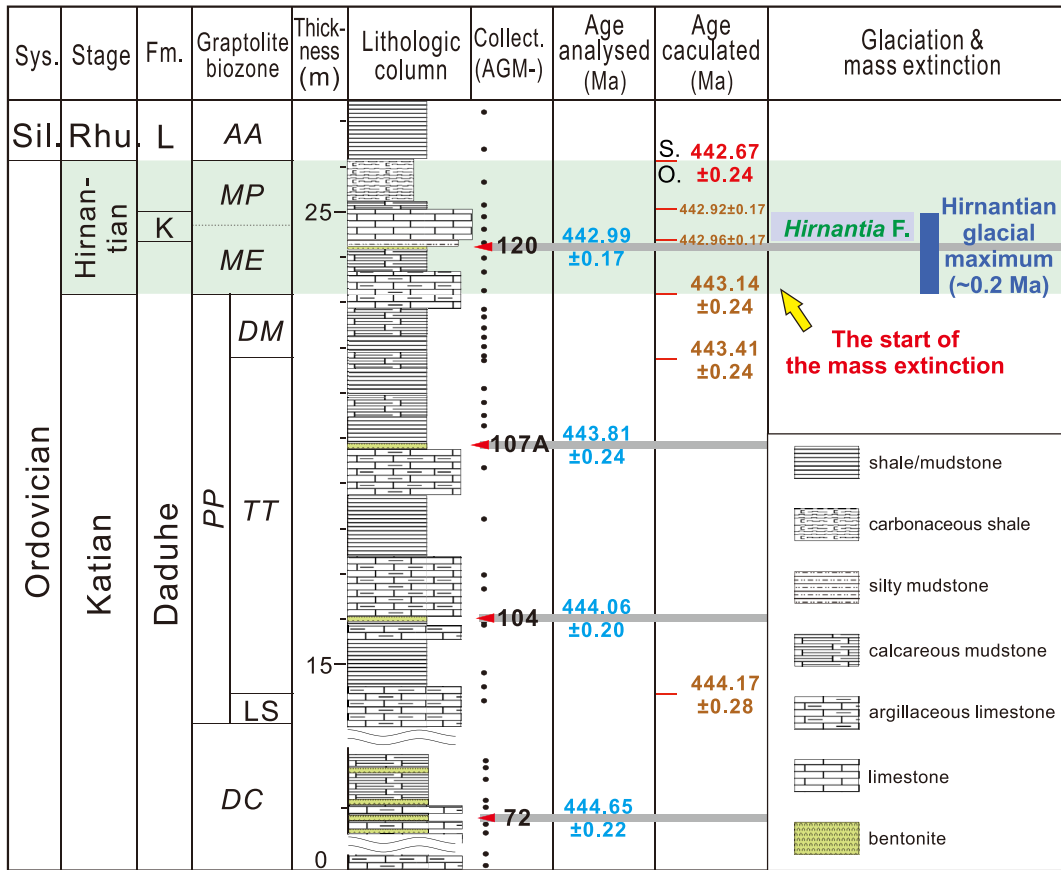


Fig. 2. Analysed or calculated $^{206}\text{Pb}/^{238}\text{U}$ ages for those key horizons at Wanhe section with indication of the end Ordovician mass extinction (EOME), the Late Ordovician glaciation, and their durations. Abbreviations: AA = *Akidograptus ascensus* Biozone; DC = *Dicellograptus complexus* Biozone; DM = *Dicellograptus mirus* Subzone; LS = Lower Subzone; ME = *Metabolograptus extraordinarius* Biozone; MP = *Metabolograptus persculptus* Biozone; PP = *Paraorthograptus pacificus* Biozone; TT = *Tangyagraptus typicus* Subzone; L = Lungmachi Formation; K = Kuanyinchiao Formation.

(3) Calculating the sedimentation rates of carbonate and mudstone/shale lithofacies for the stratigraphic interval above AGM107A. This step is based on the assumption that the ratio of sedimentation rates of limestone and mudstone remained constant in the studied stratigraphic interval (i.e., $R_{\text{lim}}/R_{\text{mud}} = 2.66$). Accumulative thickness different facies have also been included in the calculation.

$$T3_{\text{mud}}/R2_{\text{mud}} + T3_{\text{lim}}/R2_{\text{lim}} = D3$$

$$R2_{\text{lim}}/R2_{\text{mud}} = R1_{\text{lim}}/R1_{\text{mud}} = 2.66$$

where $T3_{\text{mud}}$, $T3_{\text{lim}}$ are accumulated thickness (m) of the interval for mudstone and limestone between AGM107A and AGM120, respectively. $R2_{\text{mud}}$ and $R2_{\text{lim}}$ are sedimentation rates (m/Ma) of mudstone and limestone between AGM107A and AGM120, respectively. $R1_{\text{mud}}$ and $R1_{\text{lim}}$ are sedimentation rates (m/Ma) of mudstone and limestone between AGM72 and AGM107A, respectively. $D3$ is duration (Ma) between AGM107A and AGM120.

(4) The numerical ages of major chronostratigraphic boundaries were estimated from stratigraphic thicknesses of lithofacies using the following equations:

$$A = A_0 + T_{\text{mud}}/R_{\text{mud}} + T_{\text{lim}}/R_{\text{lim}} \quad \text{or} \\ A = A_0 - (T_{\text{mud}}/R_{\text{mud}} + T_{\text{lim}}/R_{\text{lim}})$$

where A is age of the major chronostratigraphic boundaries. A_0 is ID-TIMS zircon U-Pb dates of AGM72, AGM104, AGM107A or AGM120. T_{mud} and T_{lim} is accumulated thickness (m) of the interval for mudstone and limestone. R_{mud} and R_{lim} are sedimentation rates (m/Ma) of mudstone and limestone.

Deviations of the numerical ages (A) were propagated from the deviation of ID-TIMS zircon U-Pb dates (A_0) used in the calculation and the duration of one or several intervals. Because sedimentation rate (also duration) calculation was based on serial equations and direct error propagation would yield unreal errors. The errors of the intervals were simply assumed to be the same as those of ID-TIMS zircon U-Pb dates.

6. Discussion

The base and top of the Hirnantian Stage in the latest version of the International Chronostratigraphic Chart (ICC, ver. 2019/05) are calibrated at 445.2 ± 1.4 Ma, and 443.8 ± 1.5 Ma, respectively (Fig. 4). It should be noted that

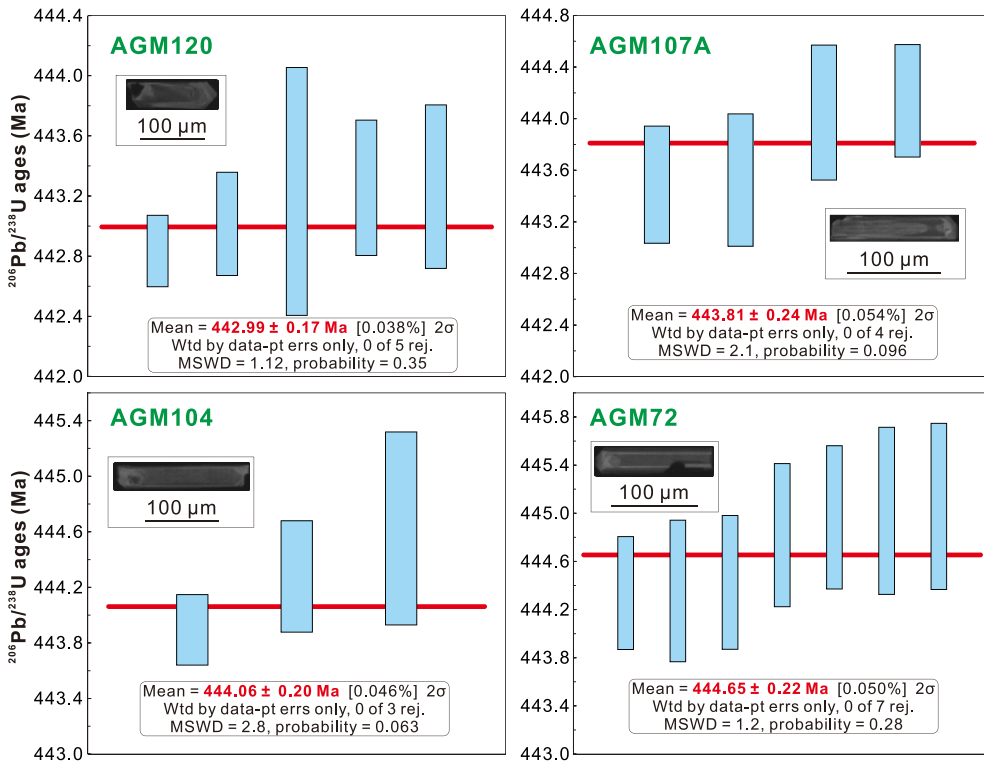


Fig. 3. Weighted mean zircon $^{206}\text{Pb}/^{238}\text{U}$ dates of the K-bentonites from the Upper Ordovician-Lower Silurian at Wanhe of Zhaotong, northeastern Yunnan Province, SW China. Representative cathodoluminescence (CL) images are presented in the diagrams.

these two ages are identical within error. The two ages were calibrated by the CONOP program using very few radiogenic isotope dates in low precision as constraining points. Furthermore, each date was yielded from multiple zircon grains, thus producing mixing dates with large uncertainties (Cooper and Sadler, 2012; Ogg et al., 2016). Among those Ordovician absolute ages, three are close to the Hirnantian Stage, one from the Upper Ordovician *P. pacificus* Biozone and the other two from the Lower Silurian *Coronograptus cyphus* Biozone and/or even slightly higher, all of which were analysed nearly thirty years ago (Tucker et al., 1990).

It should be noted that several new U–Pb dates close to the O–S boundary in South China have been obtained by different investigators. Hu et al. (2008) dated the K-bentonites from the top of the Kuanyinchiao Formation at Wangjiawan North section, the GSSP of the Hirnantian Stage, which is approximately correlated to the base of the *Metabolograptus persculptus* Biozone using SHRIMP, as 443.2 ± 1.6 Ma. Six U–Pb dates analysed by laser ablation inductively coupled plasma mass spectrometry (LA-ICP-MS) ranging from the late Katian to the early Silurian were presented at Lunshan, Jiangsu Province, eastern China (Yang et al., 2019). These dates, however, are short of robust biostratigraphic control and have much larger deviations (2.4–4.3 Ma). Due to much lower accuracy and precision relative to ID-TIMS, both SHRIMP and LA-ICP-MS are not good options to date the stratigraphic boundaries.

The four successive isotopic dates in this study from a single section ranging from the late Katian to the early

Hirnantian change the geochronology of the Hirnantian Stage in two important ways. On the one hand, the topmost of the four samples (i.e. AGM120) is from the middle *M. extraordinarius* Biozone, 1.04 m above the base of the Hirnantian Stage, while its $^{206}\text{Pb}/^{238}\text{U}$ date 442.99 ± 0.17 Ma is even 0.81 Ma younger than the age given in the ICC (ver. 2019/05) for the top of the Hirnantian. On the other hand, sample AGM107A is 3.23 m below the base of the Hirnantian Stage (upper *P. pacificus* Biozone, uppermost Katian). Its $^{206}\text{Pb}/^{238}\text{U}$ date 443.81 ± 0.24 Ma is 1.39 Ma younger than the ICC age (ver. 2019/05) for the base of the Hirnantian. As noted above, calculations in this study put the base of the Hirnantian at 443.14 ± 0.24 Ma, and its top at 442.67 ± 0.24 Ma, with a total duration of 0.47 ± 0.34 Ma for the entire stage (see Fig. 2). This suggests that the Hirnantian is significantly shorter than the previous estimation of 1.4 ± 2.05 Ma; the O–S boundary at 442.67 ± 0.24 Ma in this study is about 1.1 Ma younger than the date given in the ICC (ver. 2019/05) (Fig. 4) (Cohen et al., 2013). The new geochronologic data, therefore, provide a high-resolution geochronologic framework for the Hirnantian Stage.

One key question is the duration of the Hirnantian glaciation and its role in the EOME. The previously estimated duration of the Late Ordovician glaciation varied widely, from relatively short 1–2 Ma (Hambrey, 1985), 0.5–1.0 Ma (Brenchley et al., 1994) or 0.20 Ma (Sutcliffe et al., 2000), to a protracted >10 Ma (Saltzman and Young, 2005; Trotter et al., 2008; Elrick et al., 2013). Despite the varied estimates, however, it is now generally agreed that a glacial

Table 2
Numerical ages of major chronostratigraphic boundaries.

Stratigraphic boundaries/Samples	Distance from O–S next line (m) (m)	Thickness to next line (m)	Average sedimentation rates calculated by TIMS results			Calculated sedimentation rates by lithofacies (m/Ma)	(Ma)	Duration (Ma)	Average Sedimentation rates (m/Ma)	Numerical Deviation ages (Ma) (Ma)
			Limestone	Mudstone	Thickness Duration Sedimentation rates					
O–S boundary	0.00	0.00	1.19			12.58	4.73	0.25	4.73	442.67 0.24
Top of Hirnantia Fauna/Kuanyinchiao Fm	1.19	0.50	0.00			12.58	4.73	0.04	12.58	442.92 0.17
Base of Hirnantia Fauna/Kuanyinchiao Fm	1.69	0.00	0.12			12.58	4.73	0.03	4.73	442.96 0.17
AGM120	1.81	0.50	0.54	4.27	0.82	5.21	12.58	4.73	0.15	6.76 442.99 0.17
Base of Hirnantian/ <i>M. extraordinarius</i>	2.85	0.30	1.10				12.58	4.73	0.26	5.46 443.14 0.24
Base of <i>D. mirus</i>	4.25	0.00	1.90				12.58	4.73	0.40	4.73 443.41 0.24
AGM107A	6.08	1.00	2.64	3.72	0.25	14.88	33.45	12.58	0.25	14.56 443.81 0.24
AGM104	9.8	0.50	1.16	11.90	0.59	20.17	33.45	12.58	0.11	15.50 444.06 0.20
Base of <i>T. typicus</i>	11.45	3.28	1.52				33.45	12.58	0.22	21.93 444.17 0.28
Base of <i>P. pacificus</i>	16.35	3.10	2.25				33.45	12.58	0.27	19.71 444.38 0.31
AGM72	21.7	2.20	1.56				33.45	12.58	0.19	19.82 444.65 0.22
Base of <i>D. complexus</i>	25.46									444.84 0.31

System/Period	Series/Epoch	Stage/Age	Numerical age (Ma)	
			ICC 2019	This study
Silurian	Llandovery	Telychian		
		Aeronian		
		Rhuddanian	443.8 ± 1.5	442.67 ± 0.24
Ordovician	Upper	Hirnantian	445.2 ± 1.4	443.14 ± 0.24
		Katian		
		Sandbian		

Fig. 4. Comparison of the numerical ages of the Katian-Hirnantian boundary and Ordovician-Silurian boundary between this study and the ICC (ver. 2019/05).

maximum with an ice sheet equivalent to or exceeding the Pleistocene glacial maximum was confined to the Hirnantian (Finnegan et al., 2011), and largely within the early Hirnantian (corresponding to the *M. extraordinarius* Biozone) (Harper et al., 2014; Wang et al., 2019). The present estimate of a duration about 0.2 Ma in the lower *Metabolograptus extraordinarius* Biozone provides direct evidence of a very brief Hirnantian glacial maximum (Fig. 2), therefore supporting the belief that the severity and abruptness of the Hirnantian glaciation might be the ultimate killer of the EOME. Most of those marine organisms then diminished owing to the lack of sufficient time to adjust themselves to the extremely rapid environmental change.

7. Conclusions

High-precision isotopic dating of K-bentonite zircons from the uppermost Katian to the basal Hirnantian Daduhe

Formation (northeastern Yunnan, China) yielded four sequential $^{206}\text{Pb}/^{238}\text{U}$ dates: 444.65 ± 0.22 Ma, 444.06 ± 0.20 Ma, 443.81 ± 0.24 Ma and 442.99 ± 0.17 Ma.

Using the new isotopic dates in this study as controlling points, several key chronostratigraphic ages were calculated based on graptolite zonation and sedimentation rates at this continuous section. The base and top of the Hirnantian Stage are determined at 443.14 ± 0.24 Ma and 442.67 ± 0.24 Ma, respectively, with a duration of 0.47 ± 0.34 Ma for the stage. These ages differ significantly from 445.2 ± 1.4 Ma to 443.8 ± 1.5 Ma given in the ICC (ver. 2019/05), implying a much younger and significantly shorter Hirnantian Stage.

The early Hirnantian (*M. extraordinarius* Biozone) witnessed the Hirnantian glacial maximum. Our estimate of a duration of ~ 0.2 Ma for this time interval provides direct evidence of a brief major glaciation, supporting that the brevity and intensity of the glaciation have probably been a major killing mechanism of the EOME.

Declaration of competing interests

The authors declare that they have no known competing financial interests or personal relationships that could have appeared to influence the work reported in this paper.

Acknowledgments

S. Paxton helped with zircon separation, and S. Zink with clean laboratory and TIMS analyses. Xu Chen kindly helped identify the graptolites in this study. Financial supports for this study are from the Strategic Priority Research Program of Chinese Academy of Sciences (XDB26000000 and XDB18020102), National Key R&D Program of China (2016YFC0600408), Guangdong Natural Science Funds (2014A030306032 and 2015TQ01Z611), Youth Innovation Promotion Association of CAS (2016315) and the State Key Laboratory of Palaeobiology and Stratigraphy. This is a contribution to the IGCP Project 653 "The onset of the Great Ordovician Biodiversification Event" and No. IS-2781 from GIGCAS.

References

- Brenchley, P.J., Marshall, J.D., Carden, G.A.F., Robertson, D.B.R., Long, D.G.F., Meidla, T., Hints, L., Anderson, T.F., 1994. Bathymetric and isotopic evidence for a short-lived Late Ordovician glaciation in a greenhouse period. *Geology* 22 (4), 295–298.
- Brenchley, P.J., Carden, G.A., Hints, L., Kaljo, D., Marshall, J.D., Martma, T., Meidla, T., Nolvak, J., 2003. High-resolution stable isotope stratigraphy of Upper Ordovician sequences: constraints on the timing of bioevents and environmental changes associated with mass extinction and glaciation. *Geol. Soc. Am. Bull.* 115 (1), 89–104.
- Cohen, K.M., Finney, S.C., Gibbard, P.L., Fan, J.X., 2013. The ICS international chronostratigraphic Chart. *Episodes* 36 (3), 199–204.
- Cooper, R., Sadler, P., 2012. The Ordovician period. In: Gradstein, F.M., Ogg, J.G., Schmitz, M. (Eds.), *The Geologic Time Scale 2012*. Elsevier, pp. 489–523.
- Elrick, M., Reardon, D., Labor, W., Martin, J., Desrochers, A., Pope, M., 2013. Orbital-scale climate change and glacioeustasy during the early Late Ordovician (pre-Hirnantian) determined from $\delta^{18}\text{O}$ values in marine apatite. *Geology* 41 (7), 775–778.
- Finnegan, S., Bergmann, K., Eiler, J.M., Jones, D.S., Fike, D.A., Eisenman, I., Hughes, N.C., Tripati, A.K., Fischer, W.W., 2011. The magnitude and duration of late Ordovician–early Silurian glaciation. *Science* 331 (6019), 903–906.
- Finnegan, S., Heim, N.A., Peters, S.E., Fischer, W.W., 2012. Climate change and the selective signature of the Late Ordovician mass extinction. *Proc. Natl. Acad. Sci. U.S.A.* 109 (18), 6829–6834.
- Hambrey, M.J., 1985. The late Ordovician–early Silurian glacial period. *Palaeogeogr. Palaeoclimatol. Palaeoecol.* 51 (1), 273–289.
- Harper, D.A.T., Hammarlund, E.U., Rasmussen, C.M.O., 2014. End Ordovician extinctions: a coincidence of causes. *Gondwana Res.* 25 (4), 1294–1307.
- Hiess, J., Condon, D.J., McLean, N., Noble, S.R., 2012. $^{238}\text{U}/^{235}\text{U}$ Systematics in Terrestrial Uranium-Bearing Minerals. *Science* 335 (6076), 1610–1614.
- Hu, Y., Zhou, J., Song, B., Li, W., Sun, W., 2008. SHRIMP zircon U-Pb dating from K-bentonite in the top of Ordovician of Wangjiawan section, Yichang, Hubei, China. *Sci. China Ser. D Earth Sci.* 51 (4), 493–498.
- Huyskens, M.H., Iizuka, T., Amelin, Y., 2012. Evaluation of colloidal silicas for lead isotopic measurements using thermal ionisation mass spectrometry. *J. Anal. Atomic Spectrom.* 27 (9), 1439–1446.
- Huyskens, M.H., Zink, S., Amelin, Y., 2016. Evaluation of temperature-time conditions for the chemical abrasion treatment of single zircons for U-Pb geochronology. *Chem. Geol.* 438, 25–35.
- Jaffey, A.H., Flynn, K.F., Glendenin, L.E., Bentley, W.C., Essling, A.M., 1971. Precision measurement of half-lives and Specific activities of ^{235}U and ^{238}U . *Phys. Rev. C* 4 (5), 1889–1906.
- Jin, J.S., Zhan, R.B., Wu, R.C., 2018. Equatorial cold-water tongue in the late Ordovician. *Geology* 46 (9), 759–762.
- Ludwig, K.R., 2012. User's Manual for Isoplot 3.75: A Geochronological Toolkit for Microsoft Excel, 5. Berkeley Geochronology Center Spec. Pub., p. 75
- Mattinson, J.M., 2005. Zircon U–Pb chemical abrasion ("CA-TIMS") method: combined annealing and multi-step partial dissolution analysis for improved precision and accuracy of zircon ages. *Chem. Geol.* 220 (1), 47–66.
- Ogg, J.G., Ogg, G.M., Gradstein, F.M., 2016. *Ordovician, A Concise Geologic Time Scale*. Elsevier, pp. 57–69.
- Raup, D.M., Sepkoski, J.J., 1982. Mass extinctions in the marine fossil record. *Science* 215 (4539), 1501–1503.
- Saltzman, M.R., Young, S.A., 2005. Long-lived glaciation in the late Ordovician? Isotopic and sequence-stratigraphic evidence from western Laurentia. *Geology* 33 (2), 109–112.
- Schmitz, M.D., Schoene, B., 2007. Derivation of isotope ratios, errors, and error correlations for U-Pb geochronology using ^{205}Pb - ^{235}U - ^{233}U -spiked isotope dilution thermal ionization mass spectrometric data. *Geochem. Geophys. Geosyst.* 8 (8), Q08006.
- Sepkoski, J.J., 1996. Patterns of Phanerozoic extinction: a perspective from global data bases. In: Walliser, O.H. (Ed.), *Global Events and Event Stratigraphy in the Phanerozoic: Results of the International Interdisciplinary Cooperation in the IGCP-Project 216 "Global Biological Events in Earth History"*. Springer Berlin Heidelberg, Berlin, Heidelberg, pp. 35–51.
- Sheehan, P.M., 2001. The Late Ordovician mass extinction. *Annu. Rev. Earth Planet Sci.* 29 (1), 331–364.
- Stacey, J.S., Kramers, J.D., 1975. Approximation of terrestrial lead isotope evolution by a 2-stage model. *Earth Planet. Sci. Lett.* 26 (2), 207–221.
- Sutcliffe, O.E., Dowdeswell, J.A., Whittington, R.J., Theron, J.N., Craig, J., 2000. Calibrating the Late Ordovician glaciation and mass extinction by the eccentricity cycles of Earth's orbit. *Geology* 28 (11), 967–970.
- Tang, P., Huang, B., Wu, R., Fan, J.X., Yan, K., Wang, G., Liu, J., Wang, Y., Zhan, R., Rong, J., 2017. On the Upper Ordovician Daduhe Formation of the upper Yangtze region. *J. Stratigr.* 41 (2), 119–133 (in Chinese with English abstract).
- Trotter, J.A., Williams, I.S., Barnes, C.R., LéCuyer, C., Nicoll, R.S., 2008. Did cooling oceans trigger Ordovician biodiversification? Evidence from conodont thermometry. *Science* 321 (5888), 550–554.
- Tucker, R.D., Krogh, T.E., Ross, R.J., Williams, S.H., 1990. Time-scale calibration by high-precision UPb zircon dating of interstratified volcanic ashes in the Ordovician and Lower Silurian stratotypes of Britain. *Earth Planet. Sci. Lett.* 100 (1), 51–58.
- Villa, I.M., Bonardi, M.L., De Bièvre, P., Holden, N.E., Renne, P.R., 2016. IUPAC-IUGS status report on the half-lives of ^{238}U , ^{235}U and ^{234}U . *Geochem. Cosmochim. Acta* 172, 387–392.
- Wang, G.X., Zhan, R.B., Percival, I.G., 2019. The end-Ordovician mass extinction: a single-pulse event? *Earth Sci. Rev.* 192, 15–33.
- Yang, S., Hu, W., Wang, X., Jiang, B., Yao, S., Sun, F., Huang, Z., Zhu, F., 2019. Duration, evolution, and implications of volcanic activity across the Ordovician–Silurian transition in the Lower Yangtze region, South China. *Earth Planet. Sci. Lett.* 518, 13–25.